Supporting Information

In-Situ Construction of Titanate/Silver Nanoparticle/Titanate Sandwich Nanostructure on Metallic Titanium Surface for Bacteriostatic and Biocompatible Implants

Na Ren[a,#], *Rui Li*[b,#], *Limei Chen*[a], *Guancong Wang*[a], *Duo Liu*[a], *Yingjun Wang*[c], *Lin Zheng*[d], *Wei Tang*[d], *Xiaoqiang Yu*[a], *Huaidong Jiang*[a], *Hong Liu*[a,c,*], *and Nianqiang Wu*[b,*]

[a]State Key Laboratory of Crystal materials, Shandong University, Jinan 250100, P. R. China.

[b]Department of Mechanical and Aerospace Engineering, WVNano Initiative, West Virginia University, Morgantown, WV 26506-6106, USA.

[c]National Engineering Research Center for Tissue Restoration and Reconstruction, South China University of Technology, Guangzhou 510640, P. R. China.

[d]School of Medicine, Shandong University, Jinan 250100, P. R. China.

*To whom correspondence should be addressed. Fax: (+86) 0531-88574135. E-mail: hongliu@sdu.edu.cn, nick.wu@mail.wvu.edu

[#]contributed to the work equally

Sandwich nanostructure characterization

Six broad peaks were found in the Raman spectrum of the "Control" ample (Fig. 3a) and the detailed assignment are listed in Table S1.

Table S1. Assignments of the Raman bands in Figure 3a.

Peak (cm^{-1})	**Assignment**
193	Lattice modes and Na-O-Ti modes[1]
440	Ti-O bending vibration involving three-fold oxygen
380	Ti-O bending and stretching vibration involving two-fold oxygen
690	Ti-O bending and stretching vibration involving two-fold oxygen
810	Ti-O bending and stretching vibration involving two-fold oxygen
905	Terminal Ti-O stretching vibration involving non-bridging oxygen atoms.[1-6]

As mentioned in the context, characterizations of the nanostructure *in-situ* constructed on the titanium substrate, including SEM, HRTEM, has proved that the as-synthesized nanostructure is sodium titanate, the ion-substituted nanostructure is silver ion contained titanate, and the reduced silver-contained nanostructure is silver nanoparticle-titanate sandwich nanostructure. However, because the amount of the product layer is limited, it is difficult to confirm the precise crystalline structure of the nanostructures. Commercial titania P-25 was used as the precursor to repeat the whole reaction process of silver

nanoparticle-titanate sandwich nanostructure formation, and the powder sample thus obtained were characterized by XRD, Raman, FT-IR, and DTA/TG.

The results (Fig. S1-S4) clearly demonstrated that after each step of the preparation, the nanostructure is sodium titanate, hydrogen titanate based material plus Ag^{+}, and silver nanoparticle-hydrogen titanate sandwich nanostructure, respectively.

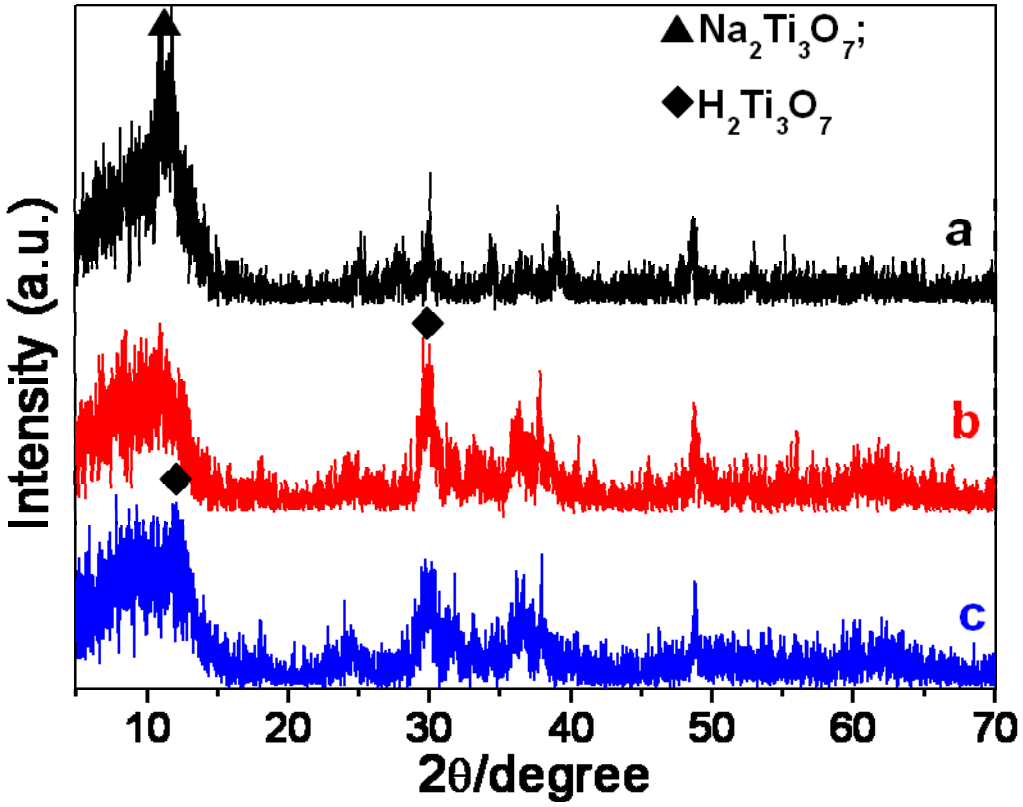

Fig. S1 XRD patterns of powder products; (a) as-synthesize titanate nanostructures by hydrothermal reaction; (b) after ion-substitution; (c) after reduction.

Although the XRD diffraction of these nanostructures in Fig. S1 is weak and the diffraction peaks are not very sharp, all diffraction peaks of as-synthesized nanostructure titanate powder (Fig. S1a) are readily indexed to the monoclinic phase of sodium titanate,

$Na_2Ti_3O_7$ (JCPDS card 31-1329), and typical (001) peak is obvious. After Ag-ion substitution, all diffraction peaks of the nanostructure (Fig. 1b) are indexed to the monoclinic phase of hydrogen titanate, $H_2Ti_3O_7$ (JCPDS card 41-192). After reduction, the peaks of the nanostructure are almost as same as those of the above-mentioned pattern, and (001) peak at 10^o becomes much higher.

Combined with the XPS results in the text, it suggests that the as-synthesized titanate nanostructure is $Na_2Ti_3O_7$, the titanate nanostructure after ion-substitution is $H_2Ti_3O_7$ with silver ions in the interlayers, and the product powder reduced by glucose should be $H_2Ti_3O_7$ with silver nanoparticles between the layers. The existence of Ag^+ in the interlayers causes the unbalance of the charge in $H_2Ti_3O_7$. Therefore, we suggest that Ag^+ in the interlayers combine with OH^- in the structure to form AgOH clusters.

Raman spectroscopy has been obtained from the above three samples to further support the above conclusion (Fig. S2). According to previous work, the bands at about 160 and 196 cm^{-1} are attributed to the Na-O-Ti bending modes.[7] The bands at about 280, 380, 428, 471, and 672 cm^{-1} are assigned to the Ti-O-Ti stretching in edge-shared TiO_6.[7-10] and the bands at about 920 cm^{-1} represent the stretching vibration of the short Ti-O bonds in distorted TiO_6 unit.[9] The bands at about 684 and 843 cm^{-1} are attributed to the $H_2Ti_3O_7$.[11,12] The highest energy mode (920 cm^{-1}) and lowest energy mode, which are assigned to the stretching of the Ti-O bonds (from distorted TiO_6 octahedron) whose oxygen is unshared, are affected by the different ions, and the wave number of this mode depends on intercalated ions. The modes, assigned as bending modes of TiO_6 octahedra (mainly involving shared oxygen atoms), are practically unchanged and they do not interact directly with intercalated ions. It can be seen

from Fig. S2a that typical bands of Na-O-Ti bending modes (160 and 196 cm^{-1}) and several bands attributed to TiO_6 layers are very clear, which demonstrates that the as-synthesized nanostructure is $Na_2Ti_3O_7$. From Fig. S2b and S2c, we can find that most peaks related to Ti-O based structure are almost the same with those in Fig. S2a. However, the typical bands of Na-O-Ti bending modes (160 and 196 cm^{-1}) disappear, and new bands at about 684 and 843 cm^{-1} attributed to the $H_2Ti_3O_7$ appear, which indicates that the main structure of ion-substituted titanate nanostructure is $H_2Ti_3O_7$. The result of Raman measurement is completely consistent with the result from XRD measurement.

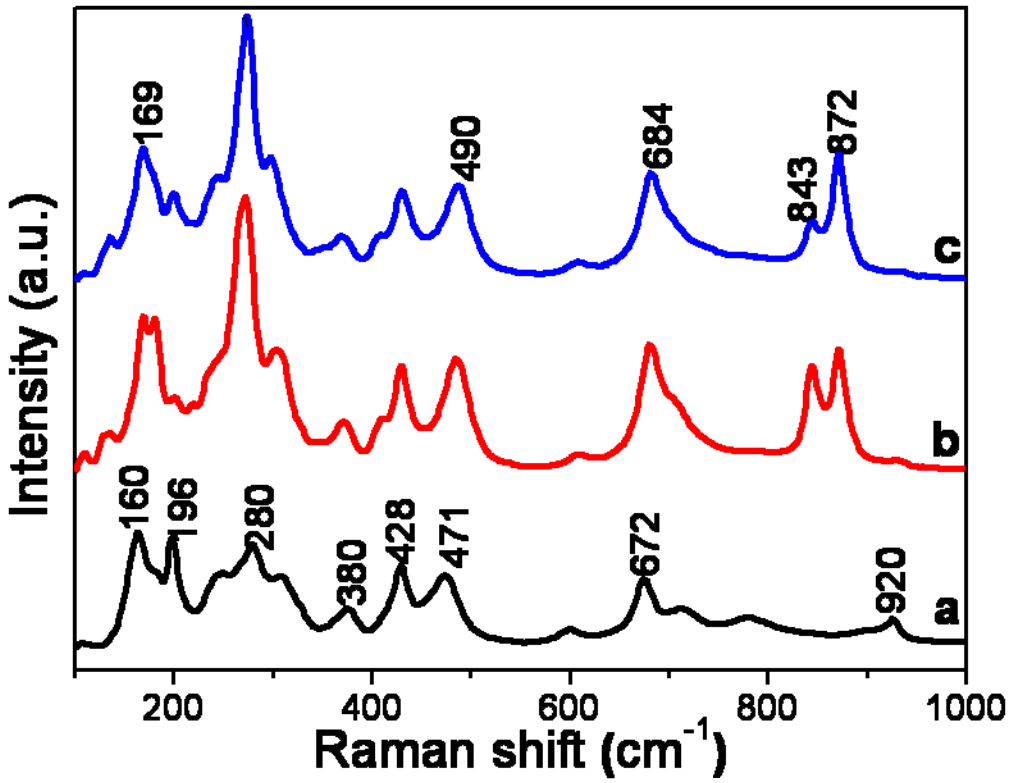

Fig. S2 The Raman spectra of the three samples; (a) sample without $AgNO_3$ solution treatment, (b) sample after $AgNO_3$ solution treatment, (c) sample after glucose solution treatment.

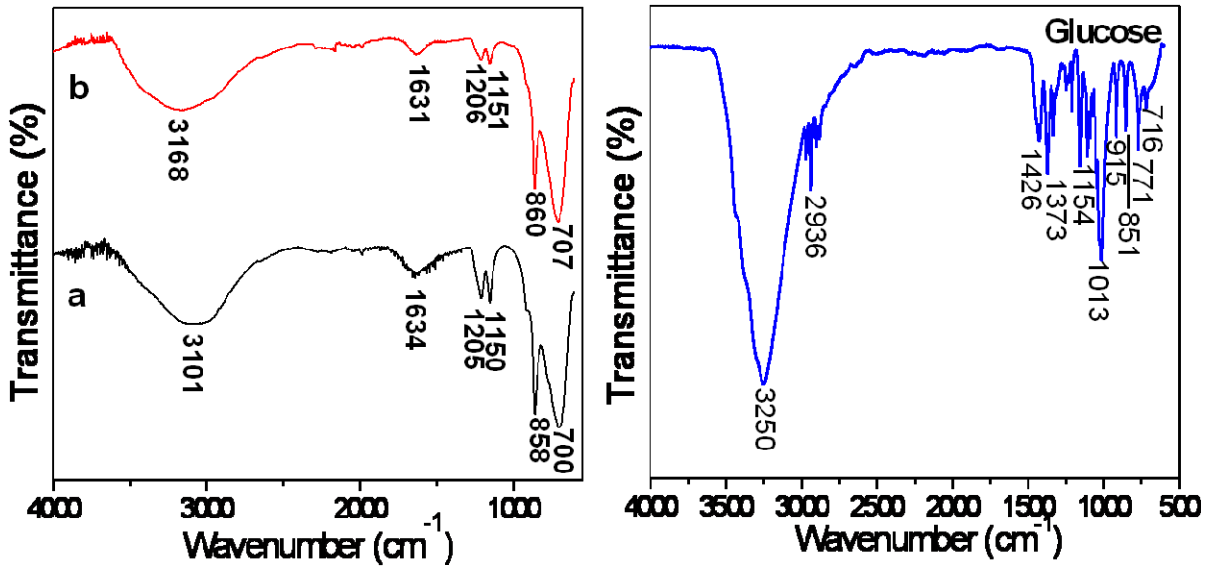

Fig. S3 IR spectra of samples before and after glucose reduction; the IR spectrum on the right belongs to glucose used.

Infrared spectra have been recorded on the ion-substituted titanate nanostrctures before and after reduction by glucose as shown in Fig. S3. It is believed that the broad peak at about 3100 and the peak at 1650 cm^{-1} correspond to the surface-adsorbed water and hydroxyl groups.[13,14] The peak at 850 cm^{-1} corresponds to the Ti-O-Ti stretching vibration of Ti ions in an octahedral coordination.[15] The spectra of the two samples are similar and possess the characteristics of $H_2Ti_3O_7$, which indicates that reduction can not affect the basic crystalline structure of ion-substituted titantate nanostructure. IR spectrum of glucose is shown in Fig. S3c. In the spectra of the both the nanostructures, no obvious band of glucose can be found, which illustrates that glucose could not be left in the interlayer after careful washing. IR measurement also supports the above conclusion.

Thermo gravimetric (TG) and Differential Thermal Analyzer (DTA) measurements have

been performed on hydrogen titanate (synthesized by immersing sodium titanate nanostructure in HCl solution)[16] and silver nanoparticle-titanate sandwich nanostructure to investigate the similarity between them, shown in Fig S4. From Fig S4a, we can see that two TG curves share very similar shape, and appear a weigh loss step between 400 and 500 ^{o}C. In Fig. S4b, a broad obvious endothermic peak appear at around 400 ^{o}C can be found on both the curves. The weight loss peak and endothermic peak are consistent with those of the typical $H_2Ti_3O_7$, which indicates that both the nanostructures are based on hydrogen titanate. The less weight loss and heat-absorption are caused by the existence of silver nanoparticle in the sandwich titanate nanostructure that could not cause weight loss and heat absorption during the calcinations process.

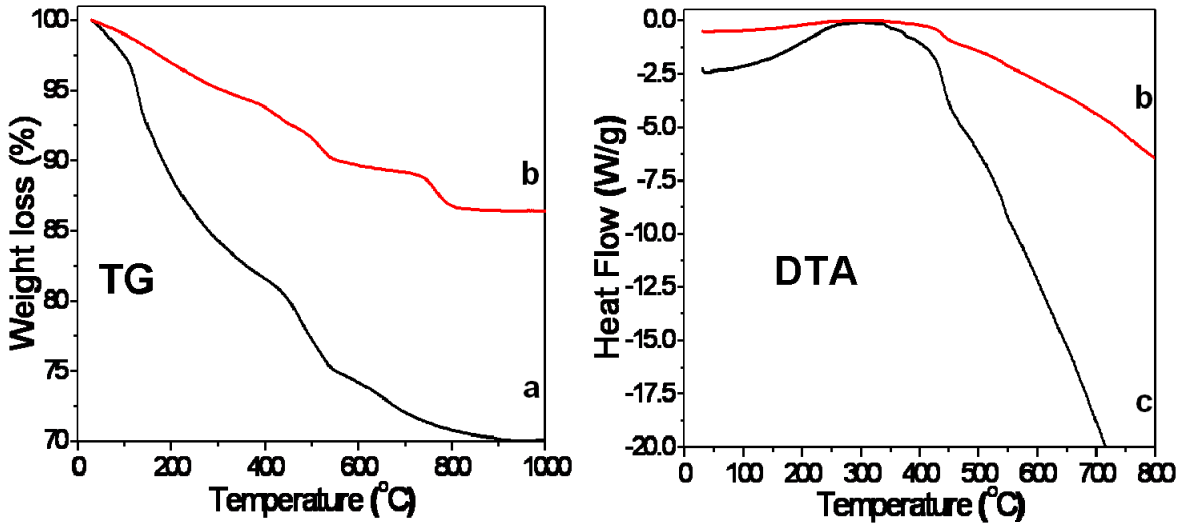

Fig. S4 TG/DTA curves of hydrogen titante nanostructure and silver-titanate sandwich nanostructure.

Ion substitution confirmation

To further demonstrate the ion substitution process, a special experiment has been designed and performed. The "Control" sample with sodium titanate nanostructure layer was immersed in silver nitrate and ultrapure water for 24 h, respectively, and the concentration of silver and sodium in silver nitrate or water before and after immersion was measured by ICP. The measurement results are shown in Table S2. The concentration of Ag^+ in $AgNO_3$ solution decreased and the concentration of Na^+ significantly increased via immersion of Ti foils with sodium titanate nanostructure, which indicates the ion substitution took place during the immersion process. After immersion of the "Control" sample in ultrapure water, no silver ions can be detected at all in the soaking liquid, but a small amount of Na ions can be observed, which indicates that sodium ions in $Na_2Ti_3O_7$ can easily release into water. This experiment proved the substitution process worked.

Table S2. The concentration changes of Ag^+ and Na^+ after immersion of sample "Control" with sodium titanate nanostructure in 0.4 mM $AgNO_3$ solution and ultrapure water, respectively (A. liquid before ion-substitution, B. liquid after ion-substitution).

	0.4 mM $AgNO_3$		**Ultrapure water**	
	Ag^+ (ppm)	Na^+ (ppm)	Ag^+ (ppm)	Na^+ (ppm)
A	38.67	0.0838	0	0
B	35	1.37	0	0.4099

Antimicrobial property

In this study, the average $N_{Control}$ is ~10^5 CFU/mL. N_{sample} for Sample "0.005mM" and "0.01mM" are less than 100, only about 1/1000 of $N_{Control}$, and the bacteridal rates of all samples are greater than 99% (Table S3), which indicates the samples after ion-substituted in

silver nitrate solution and then reduced in glucose solution, even in a very low concentration, have a very good bactericidal property. When the concentration of substitution solution is greater than 0.025 mM, the total colony number is nearly 0, which indicates that increasing the concentration of silver nitrate solution for ion-substitution reaction can improve the bactericidal ability.

Table S3. Bactericidal rates of corresponding samples.

Sample	Control	0.1mM	0.05mM	0.025mM	0.01mM	0.005mM
CFU	4.5×10^5	0	0	0	28	60
Antibacterial rate	0	100%	100%	100%	99.994%	99.987%

Long-term antibacterial ability

The "0.01mM" sample wwas immersed in PBS at 37°C for 3, 5, 7, 11, 13 days, respectively and then placed at LB agar for the zone of inhibition test.

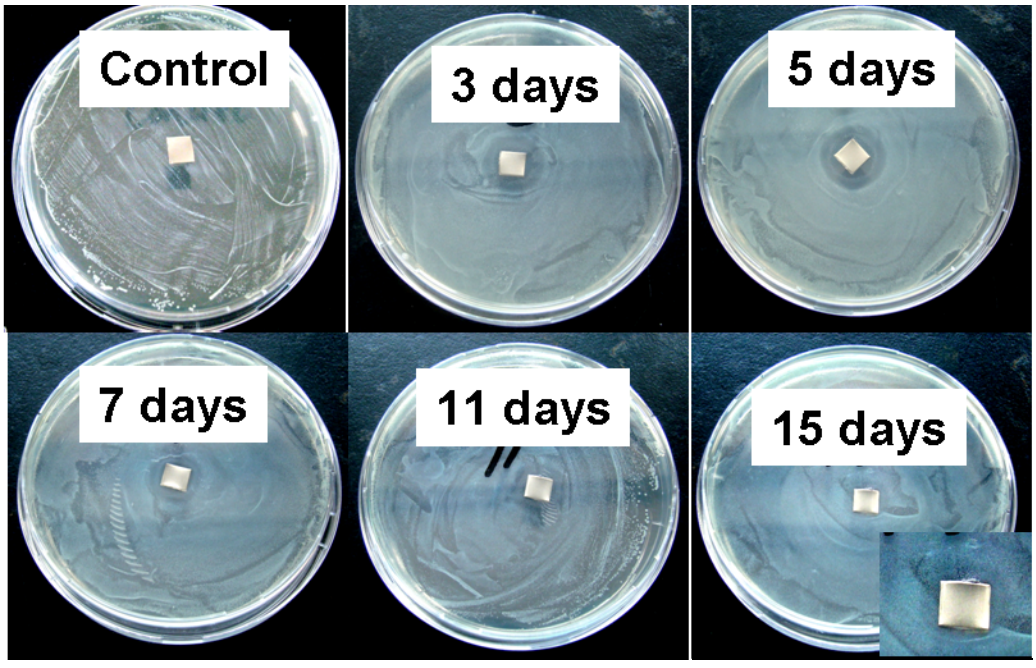

Fig. S5 Zone of inhibition test results of sample "Control" and "0.01mM" after immersion in PBS for 3, 5, 7, 11, 15 days, respectively.

Cytocompatibility Analysis

Fig. S6 shows cell proliferation on Sample "0.01mM" and "Control" for 7, 14, 21 days.

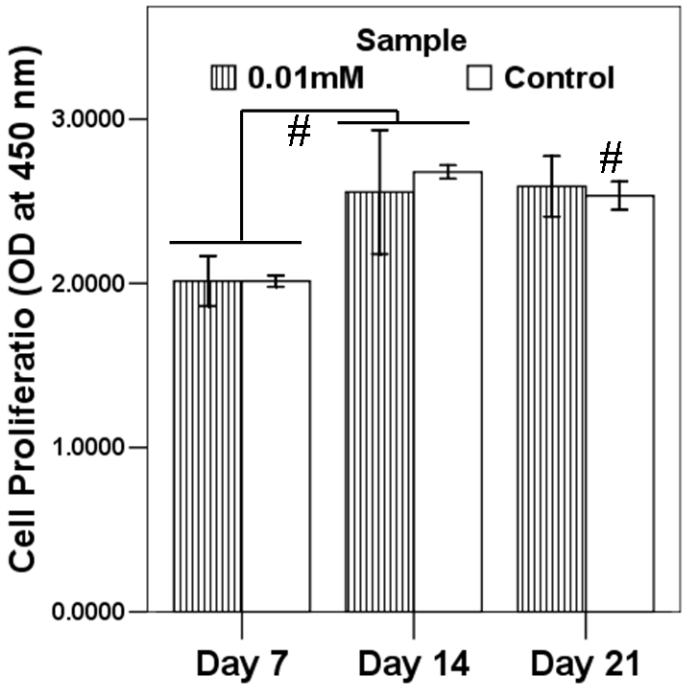

Fig. S6 Cell proliferation after culture on the samples "0.01mM" and "Control" for 7, 14 and 21 days, which was measured by CCK-8 assay. All the cell viability data were expressed as the value relative to medium without cell culture. Data are presented as mean ± standard deviation (n = 3, *p < 0.05: Ag-containing sample vs. Control; #p < 0.05: the same sample vs. the one at the previous time).

Florescence images of the nuclei of MC3T3-E1 cell cultured on the "Control" samples and the "0.01mM" sample stained with PI are shown in Fig. S7. The bright red dots represent the nuclei of the cells, which clearly display a uniform, extensive and compact distribution of MC3T3-E1 cells both on the "0.01mM" and the "Control" samples. Only a slight decrease in cell density can be observed on the Ag-loaded sample than that on the "Control".

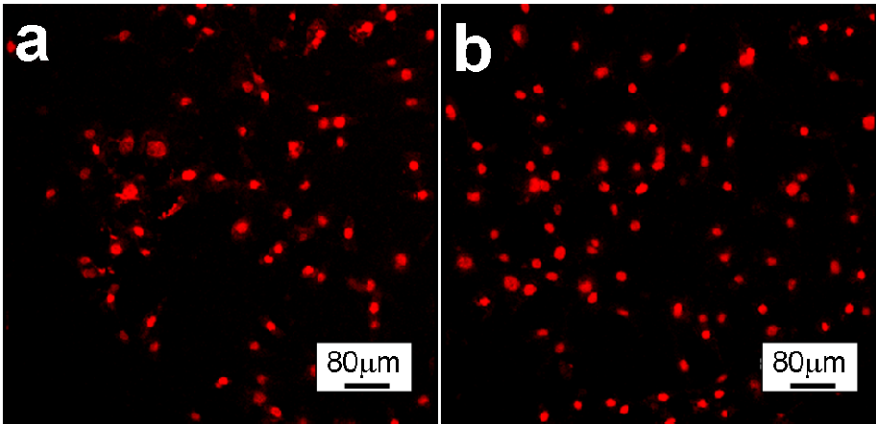

Fig. S7 Images for nucleus staining (PI) for 3 days after inoculation; (a) Cells on "0.01mM" sample, (b) cells on the "Control" sample

Fig. S8 shows the fluorescent microscope images of MC3T3-E1 cells cultured for 1, 3, 5 days on different samples, the "Control", "0.05mM", "0.01mM", "0.005mM".

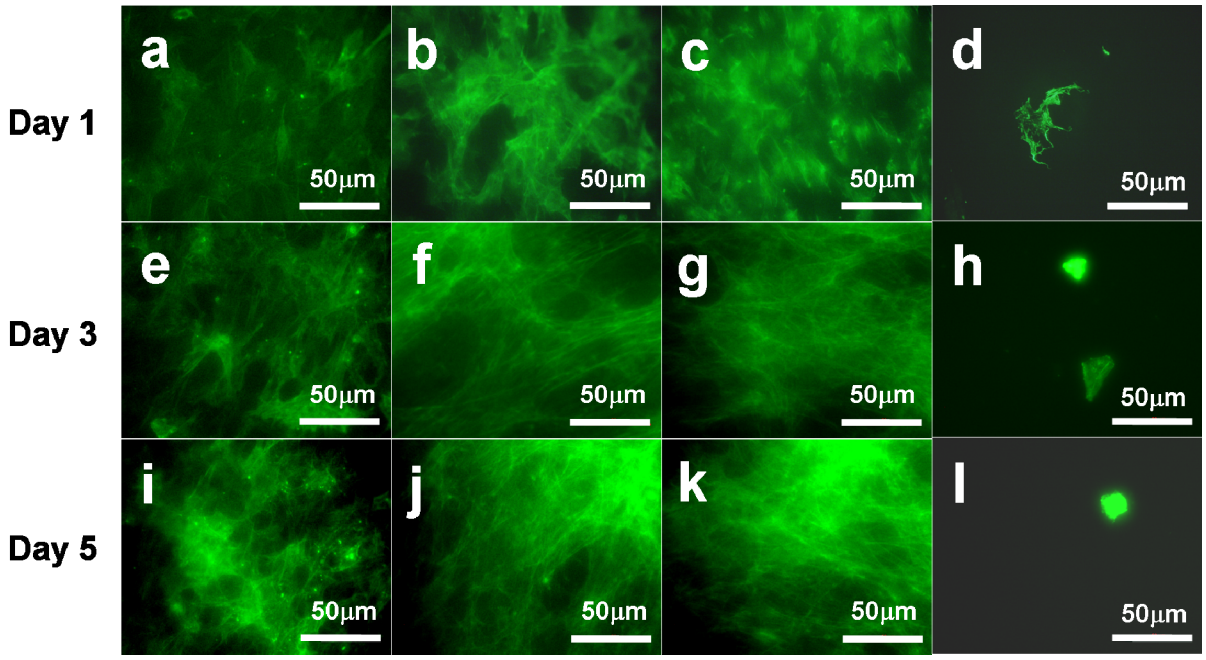

Fig. S8 Fluorescence microscopic images of cells stained with Phalloidin green cultured for 1 day on samples (a. "Control" sample; b. "0.005mM" sample, c. "0.01mM" sample, d. "0.05mM" sample, e – h. cells cultured for 3 days on those samples, i – l. cells cultured for 5 days on those samples).

Mechanism exploration

Scheme S1 depicts the biological properties (including bacteriostasis and cytocompatibility) of samples. The nanostructure of sodium titanate on the surface of Ti implants promotes the adhesion, proliferation and migration but without any antibacterial effects, while above structure suffering treatment in $AgNO_3$ solution of certain concentration and glucose solution will exert its performance on bacteriostasis and biocompatitbility.

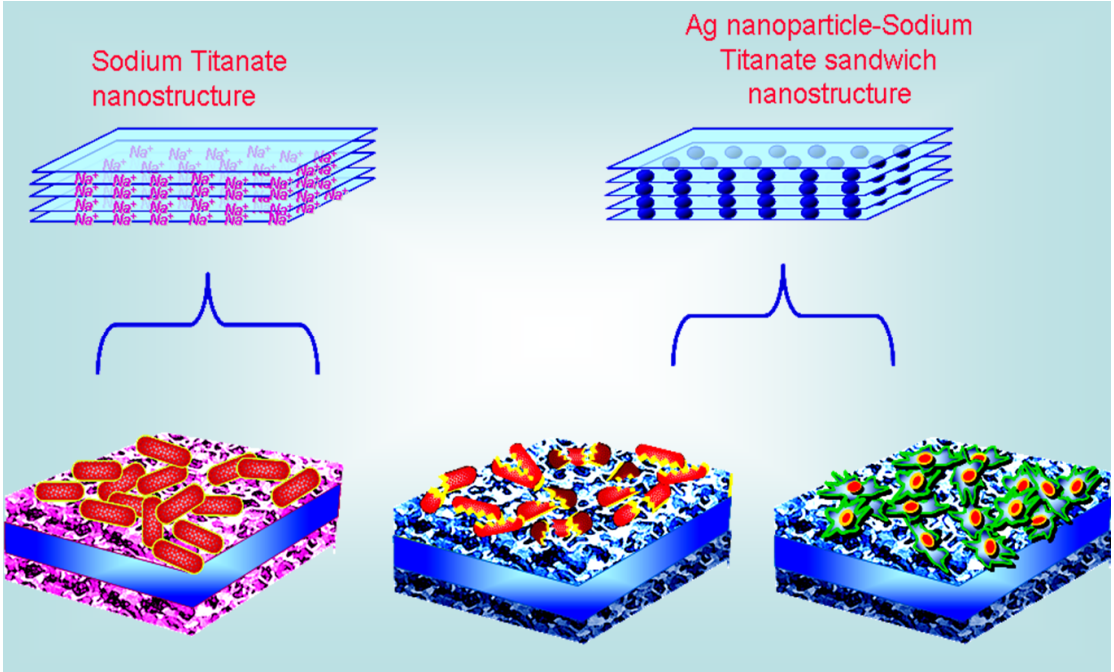

Scheme S1. The comparison of biological property for the "Control" sample and the sample with the sandwich nanostructure

References

1. Viana, B. C.; Ferreira, O. P.; Filho, A. G. S.; Filho, J. M.; Alves, O. L. Structural, Morphological and Vibrational Properties of Titanate Nanotubes and Nanoribbons. *J. Braz. Chem. Soc.* **2009**, *20*, 167-175.

2. Kim, H. M.; Miyaji, F.; Kokubo, T.; Nakamura, T. Effect of Heat Treatment on Apatite-Forming Ability of Ti Metal Induced by Alkali Treatment. *J. Mater. Sci.: Mater. Med.* **1997**, *8*, 341-347.

3. Bunker, B. C.; Peden, C. H. F.; Tallant, D. R.; Martinez, S. L.; Turner, G. L. Raman and NMR Studies of Hydrous Sodium Titanates. *Mater. Res. Soc. Symp. Proc.* **1988**, *121*, 105-109.

4. Sakka, S.; Miyaji, F.; Fukumi, K. Structure of Binary K_2O-Tio_2 and Cs_2O-TiO_2 Glasses. *J. Non-Cryst. Solids* **1989**, *112*, 64-68.

5. Miyaji, F.; Yoko, T.; Kozuka, H.; Sakka, S. Structure of $Na_2O{\cdot}2TiO_2$ glass. *J. Mater. Sci.* **1991**, *26*, 248-252.

6. Ocana, M.; Garcia-Ramos, J. V.; Serna, C. J. Low-Temperature Nucleation of Rutile Observed by Raman Spectroscopy during Crystallization of TiO_2. *J. Am. Ceram. Soc.* **1992**, *75*, 2010-2012.

7. Vianaa, B. C.; Ferreirab, O. P.; Filhoc, A. G. S; Hidalgoa, A. A.; Filhoc, J. M.; Alvesb, O. L. Alkali Metal Intercalated Titanate Nanotubes: a Vibrational Spectroscopy Study. *Vib. Spectrosc.* **2011**, *55*, 183-187.

8. Vianaa, B. C.; Ferreirab, O. P.; Filhoc, A. G. S.; Hidalgoa, A. A.; Filhoc, J. M.; Alvesb, O. L. Structural, Morphological and Vibrational Properties of Titanate Nanotubes and Nanoribbons. *J. Braz. Chem. Soc.* **2009**, *20*, 167-175.

9. Kolen'ko, Y. V.; Kovnir, K. A.; Gavrilov, A. I.; Garshev, A. V.; Frantti, J.; Lebedev, O. I.; Churagulov, B. R.; Tendeloo, G. V.; Yoshimura, M. Hydrothermal Synthesis and

Characterization of Nanorods of Various Titanates and Titanium Dioxide. *J. Phys. Chem. B* **2006**, *110*, 4030-4038.

10. Xie, J.; Ji, T. H.; Ou-Yang, X. H.; Xiao, Z. Y.; Shi, H. J. Preparation of $Srtio_3$ Nanomaterial from Layered Titanate Nanotubes or Nanowires. *Solid State Commun.* **2008**, *147*, 226-229.

11. Kőrösi, L.; Papp, S.; Csapó, E.; Meynen, V.; Cool, P.; Dékány, I. A Short Solid-State Synthesis Leading to Titanate Compounds with Porous Structure and Nanosheet Morphology. *Microporous Mesoporous Mater.* **2012**, *147*, 53-58.

12. Wei, M.; Konishi, Y.; Arakawa, H. Synthesis and Characterization of Nanosheet-Shaped Titanium Dioxide. *J. Mater. Sci.* **2007**, *42*, 529-533.

13. Yu, J. C.; Zhang, L. Z; Zheng, Z.; Zhao, J. C. Synthesis and Characterization of Phosphated Mesoporous Titanium Dioxide with High Photocatalytic Activity. *Chem. Mater.* **2003**, *15*, 2280-2286.

14. Ding, Z.; Lu, G. Q.; Greenfield, P. F. Role of The Crystallite Phase of TiO_2 in Heterogeneous Photocatalysis for Phenol Oxidation in Water. *J. Phys. Chem. B* **2000**, *104*, 4815-4820.

15. Mukhopadhayay, S. M.; Garofalini, S. H. Surface Studies of TiO_2-SiO_2 Glasses by X-Ray Photoelectron Spectroscopy. *J. Non-Cryst. Solids* **1990**, *126*, 202-208.

16. Wang, Y. M.; Du, G. J.; Liu, H.; Liu, D.; Qin, S. B.; Wang, N.; Hu, C. G.; Tao, X. T.; Jiao, J.; Wang, J. Y. *et al.* Nanostructured-Sheets of Ti-O Nanobelts for Gas Sensing and Antibacterial Applicatioins. *Adv. Funct. Mater.* **2008**, *18*, 1131-1137.